Rotor Orientation Optimization for Direct 6 Degree of Freedom Control of Multirotors

James Strawson, Pengcheng Cao, and Thomas Bewley
Dept. of Mechanical and Aerospace Engineering
University of California, San Diego
9500 Gilman Dr, La Jolla, CA 92093
{jstrawso, p5cao, bewley}@eng.ucsd.edu

Falko Kuester
Dept. of Structural Engineering
University of California, San Diego
9500 Gilman Dr, La Jolla, CA 92093
fkuester@ucsd.edu

***Abstract*—Standard multirotor designs typically arrange their propellers in the same plane, which results in an under-actuated system whose pose cannot track an arbitrary trajectory over time in 6 DoFs. Some researchers have explored 6-DoF control authority for multirotors with six or more rotors to resolve this drawback. This paper presents a multi-objective optimization (MOO) algorithm to determine the rotor tilt angles for the fixed-tilt configuration by inputting desired frame parameters and performance characteristics. While existing tilt-optimization methods seek to optimize a common inward tilt and twist for each rotor resulting in a two parameter search space, we explore an optimization method that covers independent orientation of each rotor resulting initially in 12 parameters. It then shows how the search space can be reduced to five parameters without impacting the global minimum and explore the inherent isomerism that results in the solution. The proposed objective function for the optimization is constructed to be easily understood and tuned during product design. This paper also compares the proposed optimization result with other fixed-tilt hexrotor layouts claiming to realize full actuation, and quantifies the improved control authority of the new design with experiments via both a test jig and in-flight testing.**

TABLE OF CONTENTS

1. INTRODUCTION

Multirotor unmanned aerial vehicles (UAVs) have won popularity in both commercial applications and scientific research due to their structural and operational simplicity, as well as ease of actuation [1]. They are frequently utilized due to the growing need for aerial imaging in areas of civil structures monitoring [2], ecology study [3], and cultural heritage protection [4] etc. Despite the advantages of multirotors, however, the standard multirotor designs typically employ a parallel rotor axes configuration which arranges their propellers in the same plane, resulting in an under-actuated system whose pose cannot track an arbitrary trajectory over time in 6 degrees of freedom (DoFs) [5]. The under-actuated nature of a traditional multirotor can be interpreted as its inability to exert forces parallel to its lateral plane of the body frame [6], requiring these lateral forces to be generated by rolling and pitching. In terms of aerial imaging, two- or three-axis gimbals are usually used to stabilize a camera from both vibrations and large angular motions during roll and pitch maneuvers. The mechanical and electrical gimbal designs necessary to accommodate these large disturbances consume power and add weight and complexity.

The last two decades have witnessed the innovations of researchers in multirotor designs to overcome the under-actuation drawback. In the quadcopter category, Ryll et al. [7] [8] introduced an additional set of 4 actuators to actively tilt the propellers around each of their arms in order to decouple the translational and rotational dynamics. Şenkul et al. [9] proposed the quadcopter model adding eight additional control inputs by allowing each propeller to pitch and roll in its local frame to eliminate the tilting of airframe. While in the category of multirotors with six (hexrotors) or more propellers, Kamel et al. [10] designed the Voliro hexrotor with its rotors tiltable around arms to realize full actuation, thus living up to various inspection tasks. Ryll et al. [11] [12] introduced Fast-Hex, a morphing hexrotor able to transform its configuration from under-actuated to fully actuated mode with one additional actuator. Salazar et al. [13] proposed a design with four extra lateral propellers installed at the end of each extended rotor arm of a quadcopter to produce lateral thrusts. Brescianini et al. [14] invented another eight-rotor design featuring decoupled translational and rotational dynamics and ability of omni-directional flying motion.

The aforementioned designs attempt to resolve multirotor's under-actuation by adding extra actuators either to rotate the propellers to tilt their thrust vectors or to produce lateral accelerations directly, both resulting in full- or over-actuation. These proposed ideas either increase the control complexity due to the effects of merging air flows generated by vertical and lateral rotors like in [13, 14], or result in slower system response and control challenges in real scenarios due to involving more DC motors or servomotors as rotor tilting mechanisms like in [7–12]. However, the designs of only six actuators with calculated thrust vectors in a multirotor prove to be sufficient for full actuation [5, 15, 16]. Hexrotors without rotor tilting mechanisms, which are lately categorized as fixed-tilt hexrotors [17], can provide full-actuation while keeping the actuation and construction simplicity of standard multirotors. Some researchers have already designed and validated the fixed-tilt hexrotors with optimized tilting angles for each propeller [6, 18]. However, their attempts to find the optimized rotor angles limit the search space to at most two decision variables, i.e. the cant angle and the dihedral angle applying to all propellers, and fail to search over all mounting DoFs for each rotor independently or provide independent weighting of hexacopter actuation authority in each orthogonal control direction.

This paper proposes a multi-objective optimization (MOO) approach [19] [20], which accounts for the size and mass

978-1-7281-7436-5/21/$31.00 ©2021 IEEE

distribution of a given multirotor frame. Different from [6] and [18], this method optimizes a set of six rotor orientations with a search vector related to 12 vector components to provide a desired balance of control authority over all six DoFs of the vehicle. It then shows how the search space can be reduced to 5 decision variables without impacting the global minimum and explore the inherent isomerism that results in the solution.

In an effort to focus the optimization approach towards airframe designers and engineers, the formulation of the proposed optimization approach allows a user to tune the relative weights assigned to the control authority in each of the six orthogonal independently in positive and negative directions for specific applications. The optimization approach also incorporates the practical limits of unidirectional motor control and the mixing-matrix method to multirotor flight control which is commonplace in commercial flight controllers. The proposed approach is used to optimize a hexrotor design case study which is subsequently built, tested, and flown to demonstrate the validity of the approach.

The focus and structure of this paper is therefore: *(i)* to define and derive the airframe layout, rotor orientations, force and mixing matrices, and control authority vectors in Sec.§2, *(ii)* to devise the MOO optimization algorithm and present the result of a hexrotor case study in Sec.§3, *(iii)* to compare the case study result with peers' configurations in Sec.§4, *(iv)* to present approach and results of motor-propeller characterization, the experimental hexrotor test stand and in-flight lateral thrusts measurements of the case study in Sec.§5, *(v)* to come to conclusions and articulate future perspectives in Sec.§6.

2. QUANTIFYING PERFORMANCE

The section defines and derives a sequence of definitions and performance metrics for a set of rotor orientations based on a weighted sum of the available control authority about and along each axis. We define the control authority as the available forces and torques of the system when control inputs are applied independently while in an equilibrium hover state. This takes into account the upper and lower limits of individual motors inputs. Different weights may be placed on the positive and negative directions for each of the six control directions.

Frame Layout Definition

This paper uses the convention of centering a NED coordinate body frame at the center of mass of the multirotor, with Z pointing out the bottom of the frame, X pointing forward, and Y pointing to the right. Roll, pitch, and yaw angular directions follow the right-hand rule about X, Y, and Z respectively. All forces in this paper are reported in Newtons, with moments in Newton meters, and angles in radians. More details of the body frame definition are visualized in Fig. 1 and Fig. 2.

The center of pressure on each of the propellers is assumed to be in the centroid of the propeller itself, with the applied force acting colinearly with the rotor axis. It is important to design and construct the frame by locating the centroids of the propellers themselves, not the motor mount bases. The positions of the six propeller centroids relative to the center of mass of the frame are given by three vectors:

$$\begin{aligned} c_x &= [0.179, 0, -0.179, -0.179, 0, 0.179], \\ c_y &= [0.104, 0.207, 0.104, -0.104, -0.207, -0.104], \\ c_z &= -[0.0307, 0.0307, \ldots, 0.0307]. \end{aligned} \quad (1)$$

For our case study, the propeller positions form an evenly spaced circle in a plane 30.7mm above the center of mass as derived from our CAD model; the majority of existing multirotor frames implement such evenly spaced arrangements. However, the method described here accommodates much more general arrangements of the rotors, including asymmetric layouts. In section 2, it is shown that controllability of a particular configuration can be verified by ensuring that the system's force matrix has full rank. A less common V-style hexrotor arrangement, popular for supporting wide camera angles, is suitable in this regard, and can benefit significantly from the optimization method suggested herein.

The layout of the case study considered in this work is shown in top, back, and isometric views in Fig.1. Note that the six rotors are indexed clockwise about the origin starting at the front right. The body frame of the hexrotor is also marked in the figure with the NED convention.

Rotor Orientation Definition

Since the the force generated by each propeller is assumed to be applied to the propeller's physical centroid, it is convenient to define the orientation of each rotor axis as a unit vector starting at the propeller centroid location and extending in the direction of the force applied by the propeller. Each rotor then has two degrees of freedom to be optimized, namely, the tilt in the X and Y directions from a nominal vertical orientation. For a 6-rotor hexrotor frame, this results in 12 parameters to optimize over. The X and Y components of these six unit vectors relative to their origin are organized into two vectors v_x and v_y. If v_x and v_y contained all zeros, then all rotors would be pointing upwards in the negative Z direction. An example of the 2-DoF rotor orientation vector is given as:

$$V_1 = [v_x^1, v_y^1, v_z^1] = [-0.173, 0.233, -0.957] \quad (2)$$

The corresponding six components in the Z direction of the unit force vectors are organized in v_z. Since v_z is derived from the x and y components it cannot be manipulated while optimizing and is not part of the search space. However, it is used when constructing the force matrix.

Force Matrix and Vectors

The 6×6 force matrix F defines the contributions from each rotor to each of the three forces and three moments on the body. Representing this matrix accurately requires experimentally-derived properties of the motor and propeller combination (the rotor), specifically the maximum thrust T_{max} and maximum drag torque $\tau_{d,max}$ that each rotor generates under steady load. The vast majority of commercial motors and propellers in the multirotor industry today are unidirectional, so they can be said to accept a normalized control input u from 0 (off) to 1 (max), where a positive control input u_i of 1 to each rotor generates a positive steady-state thrust force and drag torque of T_{max} and $\tau_{d,max}$, which are obtained using the methods mentioned in Sec.§5. For our case study, these maximum values and the total mass of the aircraft m_f are:

(a) (b) (c)

Figure 1. **CAD rendering of the airframe used in the case study, showing the coordinate system and rotor indexing.**

$$T_{max} = 4.72\,N,\ \tau_{d,max} = 0.0775\,Nm,\ m_f = 0.992\,kg. \tag{3}$$

And utilizing the mass property simulation from the CAD rendering in Fig. 1, we can estimate the moments of inertia about 3 principal axes of the body frame:

$$\begin{aligned} I_{xx} &= 8.44 \times 10^{-3}\,kg \cdot m^2, \\ I_{yy} &= 8.19 \times 10^{-3}\,kg \cdot m^2, \\ I_{zz} &= 1.40 \times 10^{-2}\,kg \cdot m^2, \end{aligned} \tag{4}$$

There is freedom in the mechanical design to choose the rotation direction of each rotor; these directions are summarized here as rotation vector r with entries of -1 indicating clockwise rotation, and $+1$ indicating counterclockwise rotation when viewed from above. While the motor torques on the frame are small as compared with the moments generated by the rotor thrusts, they are not negligible and it is shown in Sec.§3 that reversing the propeller spin directions can in some cases flip the optimized orientation of the rotors. For our case study, we use a typical hexrotor rotation pattern given by:

$$r = [1, -1, 1, -1, 1, -1] \tag{5}$$

The force matrix F can now be constructed by listing the the force and torque component generated by each rotor along and about each body axis. Each row i corresponds to contributions from an individual rotor and the columns are the resulting forces and moments (in units of N and Nm) resulting from a unit control input to rotor i. This matrix is defined, in the case of six rotors, as follows.

$$F = \begin{bmatrix} f_x^1 & f_y^1 & f_z^1 & \tau_{roll}^1 & \tau_{pitch}^1 & \tau_{yaw}^1 \\ f_x^2 & f_y^2 & f_z^2 & \tau_{roll}^2 & \tau_{pitch}^2 & \tau_{yaw}^2 \\ f_x^3 & f_y^3 & f_z^3 & \tau_{roll}^3 & \tau_{pitch}^3 & \tau_{yaw}^3 \\ f_x^4 & f_y^4 & f_z^4 & \tau_{roll}^4 & \tau_{pitch}^4 & \tau_{yaw}^4 \\ f_x^5 & f_y^5 & f_z^5 & \tau_{roll}^5 & \tau_{pitch}^5 & \tau_{yaw}^5 \\ f_x^6 & f_y^6 & f_z^6 & \tau_{roll}^6 & \tau_{pitch}^6 & \tau_{yaw}^6 \end{bmatrix} \tag{6}$$

Since the rotor orientations are defined as unit vectors, we can sum together the components of each rotor's force and moment in each direction to construct the entries of the force matrix F. This may be extended to larger numbers of rotors by adding additional rows to F. We denote T_i and τ_d, i to be the thrust force and drag torque of the i-th propeller, respectively, and find:

$$\begin{aligned} f_x &= \sum_{i=1}^{6} f_x^i = \sum_{i=1}^{6} v_x^i T_i \\ f_y &= \sum_{i=1}^{6} f_y^i = \sum_{i=1}^{6} v_y^i T_i \\ f_z &= \sum_{i=1}^{6} f_z^i = \sum_{i=1}^{6} v_z^i T_i \\ \tau_{roll} &= \sum_{i=1}^{6} \tau_{roll}^i = \sum_{i=1}^{6} (c_z^i v_y^i - c_y^i v_z^i) T_i - \tau_{d,i} r^i v_x^i \\ \tau_{pitch} &= \sum_{i=1}^{6} \tau_{pitch}^i = \sum_{i=1}^{6} (c_x^i v_z^i - c_z^i v_x^i) T_i - \tau_{d,i} r^i v_y^i \\ \tau_{yaw} &= \sum_{i=1}^{6} \tau_{yaw}^i = \sum_{i=1}^{6} (c_x^i v_y^i - c_y^i v_x^i) T_i - \tau_{d,i} r^i v_z^i. \end{aligned} \tag{7}$$

In (7), each component of the 6-DoF wrench in the body frame is constructed over the summations of vectored thrusts and torques of each rotor. In the scope of this paper, we ignore the gyroscopic and inertial effects induced by the motors and propellers [6], since both can be considered as second-order disturbances and rejected by feedback controllers to be designed in our future work. As two outputs of optimization algorithm discussed later, the f_{min} and f_{max} vectors therefore deliver the desired minimum and maximum total forces and torques, respectively, to be exerted on the hexrotor center of mass as shown in (8).

$$\begin{aligned} f_{min}(v^1, \ldots, v^6) &= min([f_x, f_y, f_z, \tau_{roll}, \tau_{pitch}, \tau_{yaw}]) \\ f_{max}(v^1, \ldots, v^6) &= max([f_x, f_y, f_z, \tau_{roll}, \tau_{pitch}, \tau_{yaw}]) \end{aligned} \tag{8}$$

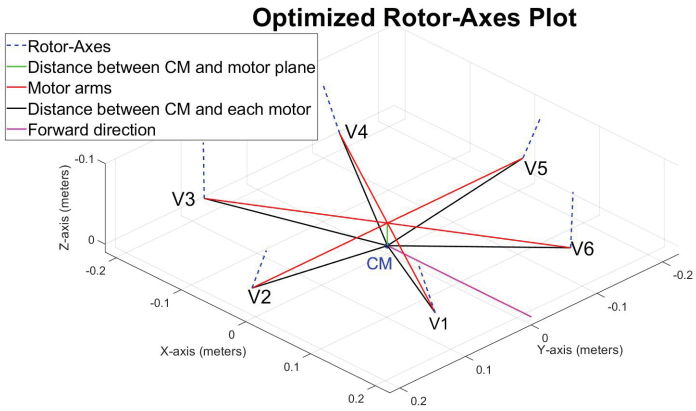

Figure 2. The geometric representation of an optimized axes layout in the body frame showing the origin and coordinate system.

Mixing Matrix

The next step is to construct a mixing matrix which will be used in the implemented flight controller. Mixing is the process of generating individual control signals to each of the rotors which result in orthogonal control inputs along and about the three axes [21]. This allows SISO feedback controllers to be used for each of the orthogonal degrees of freedom [22]. For a linear control model, each SISO controller's output is mixed to generate signals to all six rotors.

The first step is to take the inverse of the force matrix F, which is only possible when it is square and full-rank. To extend this method to non-square F (more than six rotors), it is possible to use the pseudoinverse.

Second, a diagonal matrix with d_1 through d_6 is left multiplied with the inverse of F matrix to obtain a scaled matrix M. d_1 through d_6 are chosen to scale the rows of M in such a way that a control input of $+1$ or -1 in any given direction saturates at least one of the motor inputs on its upper or lower bound during steady equilibrium hover conditions. This is done to ensure that the outputs of the SISO feedback controller are scaled appropriately when implemented. To accomplish this, it is necessary to find what inputs to the motors are required for an equilibrium hover state. This will vary with different payloads, and even different levels of battery charge for a given payload, so a nominal condition is chosen with the battery at half-charge and the mass of a typical payload included with the mass of the frame.

$$M = \begin{bmatrix} d_1 & & \\ & \ddots & \\ & & d_6 \end{bmatrix} F^{-1} = \begin{bmatrix} m_x^1 & \dots & m_x^6 \\ m_y^1 & \dots & m_y^6 \\ m_z^1 & \dots & m_z^6 \\ m_{roll}^1 & \dots & m_{roll}^6 \\ m_{pitch}^1 & \dots & m_{pitch}^6 \\ m_{yaw}^1 & \dots & m_{yaw}^6 \end{bmatrix} \quad (9)$$

As the center of mass is at the origin of the coordinate system, the condition for steady hover is that the hexrotor is only exerted with the gravitational force of $9.81 \cdot m_f$ N in the Z direction at the origin, and zero forces and moments in the remaining directions. The motor control signals s_h required for steady hover may be found by solving the linear system in (10a) with the solution for our case study given by (10b):

$$f_h = F^T s_h = [0, 0, 9.81 m_f, 0, 0, 0]^T, \quad (10a)$$

$$\Rightarrow \quad s_h = [0.364, 0.364, 0.364, 0.364, 0.364, 0.364]^T. \quad (10b)$$

This result shows that the optimized case given in (22) requires 36.4% throttle from all motors to hover. This is a result of the radially symmetric frame layout. Note that the property of requiring equal throttle across all motors for steady hover is observed for symmetric frame layouts, and when a global minimum has been reached during the optimization. Other valid and usable rotor orientations do not necessarily exhibit this property.

Thirdly, each row of the mixing matrix is scaled such that, when any single minimum or maximum control force or torque is applied during steady-state hover, no motor control signal s_i exceeds the range $[0, 1]$. In those asymmetric directions, which are X and pitch in our case, it is likely that one direction may allow more control authority than the other. Thus, the rows of the mixing matrix are scaled such that the direction allowing greater control authority saturates a motor when a control input of -1 or $+1$ is applied. The choice of control input range from -1 to $+1$ only serves to scale the mixing matrix for convenience of implementation, and does not affect the results of this optimization.

Control Force Authority Vectors

Finally, we create two vectors f_{min} and f_{max} of the forces (in N) and moments (in Nm) that result from applying the minimum and maximum control inputs to each channel independently. To find these, first we construct two vectors u_{min} and u_{max} consisting of the saturation limits found during the mixing matrix scaling operation, as shown in (9):

$$\begin{aligned} u_{min} &= [-0.57, -1.0, -1.0, -1.0, -0.93, -1.0], \\ u_{max} &= [1.0, 1.0, 0.0, 1.0, 1.0, 1.0]. \end{aligned} \quad (11)$$

To find the forces generated by these control limits, simply left multiply the control inputs u_{min} and u_{max} by the force and mixing matrices. Note that, due to (9), this can be reduced to multiplying by the row scaling factors d_1 through

d_6.

$$f_{min} = F^T M^T u_{min} = \begin{bmatrix} d_1 & & \\ & \ddots & \\ & & d_6 \end{bmatrix} u_{min}^T,$$
$$f_{max} = F^T M^T u_{max} = \begin{bmatrix} d_1 & & \\ & \ddots & \\ & & d_6 \end{bmatrix} u_{max}^T. \quad (12)$$

Note specifically that these are the minimum and maximum *total* forces and torques applied by the rotors to the aircraft with the optimized configuration illustrated in Fig. 4; the value of f_h required to maintain hover, as given in (10a), is $g\,m_f = 9.74\ N$ in the third component and zero in the other components. Note that, due to the symmetry of the frame, the control authority of translation along Y-axis and rotations about X and Z-axis are symmetric, but the authority in the other directions are not. It is discussed in Sec.§3 how the control authorities are manipulated.

3. Optimization Approach

The proposed optimization approach, which is named as "Optimum" in this paper, is based on an application of the multi-objective optimization (MOO) method. The weights in our objective function are selected to suit the requirements for an indoor airborne image sensor. Similar to the approaches in [6] and [18], We also constrain the search space as appropriate, in order to search quickly for the optimum set of orientations. The optimization codes are composed in MATLAB, and they are available on the author's github page: `https://github.com/StrawsonDesign/multirotor_angle_optimizer`.

Search Space

For an arbitrary rotor specification and layout in the NED body frame, each normalized rotor-axis vector will be determined by 2 degrees of freedom (X and Y components), and the Z component comes from the constraint of unit vector. Thus there are 12 parameters in the search space assuming the rotor rotation directions are fixed by practical design rules and design choice. In this case study, we choose to give symmetric weighting on control authority in the left and right direction, thus the frame can be restricted to be symmetric from left to right. More specifically, the rotor positions and orientations of rotors 1, 2, and 3 are mirrored across the XZ plane to define rotors 4, 5 and 6. This reduces the search space to 6 variables.

For the multirotor to hover still with equal thrust applied to all rotors, the sum of forward-facing X components of all rotors must also equal 0 by observation. Running the optimization routine practically demonstrates that this condition is met at the global minimum. The same is automatically true in the Y direction due to the mirror constraint mentioned earlier,

$$0 = \sum_{n=1}^{6} v_y^i, \quad 0 = \sum_{n=1}^{6} v_x^i. \quad (13)$$

This property can be exploited to reduce the search space further to only 5 variables by imposing these sums, as well as the symmetry across the XZ plane, as constraints. The search vector p can thus be defined as the following orientation components of rotors 1 through 3.

$$p = [v_x^1, v_y^1, v_x^2, v_y^2, v_y^3] = [p_1, p_2, p_3, p_4, p_5]. \quad (14)$$

From this reduced search space, we can still populate the other rotor orientation vector components by imposing the symmetry and the sums constraints in (13),

$$\begin{gathered} v_x^6 = v_x^1,\ \ v_x^5 = v_x^2,\ \ v_x^4 = v_x^3,\ \ v_x^3 = -(v_x^1 + v_x^2) \\ v_y^6 = -v_y^1,\ \ v_y^5 = -v_y^2,\ \ v_y^4 = -v_y^3. \end{gathered} \quad (15)$$

Objective function and weights

We define the criterion for the optimization as the minimization of a scalar objective function J. We propose a linear weighted sum of the components of f_{min} and f_{max} such that

$$J = \sum_{n=1}^{6} w_{min} \cdot f_{min} - \sum_{n=1}^{6} w_{max} \cdot f_{max}. \quad (16)$$

For this study, based on our desired flight characteristics, we choose the weights for this expression to be:

$$\begin{aligned} w &= [w_x, w_y, w_z, w_{roll}, w_{pitch}, w_{yaw}], \\ w_{min} &= [10, 12, 40, 2, 2, 5], \\ w_{max} &= [20, 12, 0, 2, 2, 5]. \end{aligned} \quad (17)$$

The resulting frame is intended for use as an indoor imaging platform, and therefore the emphasis is placed on the Z-component in w_{min} to obtain considerable hover thrusts, and X-component in w_{max} for forward flight purpose. For the three angular directions, it is desired to be able to turn about the yaw axis quickly, so a higher weighting is placed on the yaw torque rather than the roll and pitch torques. These weights are intentionally constructed to allow engineers and designers to intuatively tune control authority for practical designs.

Global Minimum Computation

We need to find the constraints for our search space. Since the unit vector components are derived from p, the range of possible starting points must be carefully selected by constraining the five components of p as follows to avoid rotor orientation vectors with length > 1.

$$1 > p_1^2 + p_2^2, \quad 1 > p_3^2 + p_4^2, \quad 1 > p_5^2 + (p_1 + p_3)^2. \quad (18)$$

We will also need to examine the relationship between the weight and the maximum vertical lift which is represented by $f_{min}[3]$ in our scope. Given the fact that curve of our input motor signals vs output thrusts is roughly linear as indicated in Fig. 9, in order to lift the hexrotor at 40% battery level (e.g. 15.2V for a 4S 14.8V battery) during the flight, we set the weight of the hexrotor to be less than or equal to 40% of the total maximum vertical thrusts. The corresponding constraint is derived as follows:

$$\begin{gathered} \sqrt{(1 - p_1^2 - p_2^2)} + \sqrt{(1 - p_3^2 - p_4^2)} + \\ \sqrt{(1 - p_5^2 - (p_1 + p_3)^2)} \geq 0.2 \frac{g\,m_f}{T_{max}} \end{gathered} \quad (19)$$

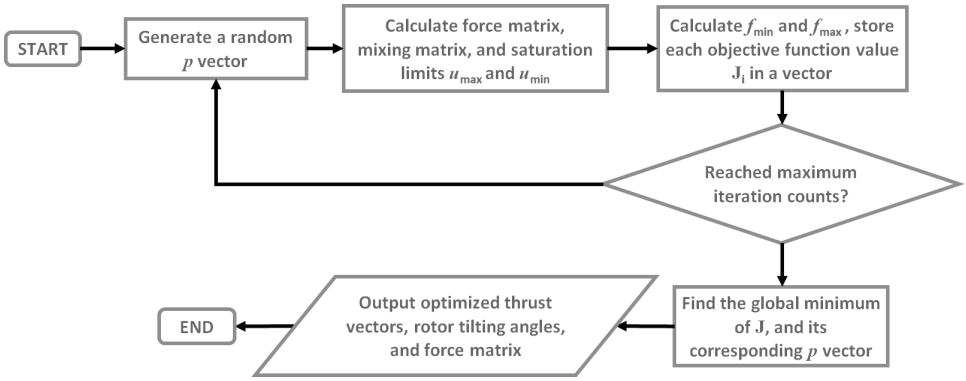

Figure 3. **The flowchart of the proposed MOO optimizer for rotor orientations.**

In our case study, in order to satisfied the aforementioned lift requirement for a multirotor mass of $m_f = 0.992\,kg$, we must have our results satisfy $f_{min}[3] \leq -24.329N$.

Incorporating all the constraints and the objective function, we thus define the optimization problem as:

$$\underset{p\in \mathrm{R}^5}{\text{Minimize}} \sum_{n=1}^{6} w_{min} \cdot f_{min} - \sum_{n=1}^{6} w_{max} \cdot f_{max}. \tag{20}$$

subject to

$$\begin{aligned} p_1^2 + p_2^2 &< 1, \\ p_3^2 + p_4^2 &< 1, \\ p_5^2 + (p_1 + p_3)^2 &< 1, \\ \sqrt{(1 - p_1^2 - p_2^2)} + \sqrt{(1 - p_3^2 - p_4^2)} + & \\ \sqrt{(1 - p_5^2 - (p_1 + p_3)^2)} &\geq 0.2 \frac{g\, m_f}{T_{max}}. \end{aligned} \tag{21}$$

Due to the nonlinear saturation process in constructing the mixing matrix, the search space is littered with local minima and often fails to converge for unreasonable starting points. Since this computation is not intensive, the global minimum can easily be found by starting Matlab's *fminsearch* function [23] at evenly spaced starting points across the search space. The algorithm flowchart of the optimizer program is shown in Fig. 3.

Optimized Result of a Hexrotor Case Study

In (22), the components of optimized rotor axes vectors and the corresponding f_{min} and f_{max} vectors for a hexrotor case study are presented. Apart from the optimization scheme, this hexrotor configuration is also determined by the length of rotor arms and potitions of each propeller centroid in the body frame. Fig. 4 gives the result plot of the case study layout. The central red line segment indicates the forward flight direction by pointing out positive X-direction of the vehicle body frame, and the other red line segments indicate the rotor arms with shorter blue line segments indicating the X and Y components of the optimized rotor axes locating at each far end of arms. The "Vertical Thrust Effectiveness" (abbreviated to VTE) in Fig. 4 represents the percentage of total thrust that is in Z-direction at steady hover state, while the "Hover Throttle" is the throttle needed to lift the hexrotor when hovering. These results are later compared with configurations by other researchers in Sec.§4, and validated in Sec.§5.

$$\begin{aligned} v_x &= [-0.173, 0.391, -0.218, -0.218, 0.391, -0.173], \\ v_y &= [0.233, 0.031, -0.195, 0.195, -0.031, -0.233], \\ v_z &= -[0.957, 0.920, 0.957, 0.957, 0.920, 0.957]. \\ f_{min} &= [-1.99, -1.45, -26.7, -1.14, -1.11, -0.51]^T, \\ f_{max} &= [3.49, 1.45, 0, 1.14, 1.20, 0.51]^T. \end{aligned} \tag{22}$$

Isomerism in Solution

Due to the left/right mirror symmetry across the XZ plane imposed by the orientation constraints, there are two easily observable isomers in the solution set which are mirrors of each other across the YZ plane. The isomer of the original solution from Fig.4 can be seen in Fig.5 which displays an identical performance metric but with reversed control authority vectors. This can be generated by reversing the rotor rotation directions and flipping w_{min} and w_{max} in all directions but Z.

The available thrust in the forward X direction is the most heavily asymmetric control authority so one isomer can be reliably chosen over another by making the X direction weighting asymmetric. This would likely be done to conform to aesthetic or mechanical design constraints, or simply to favor steady forward flight over backward flight.

The motor torque applied to the frame is quite small compared with the moments generated by the rotor thrust, but given symmetric weightings w_{min} and w_{max} a reversal of all rotor spin directions will result in an optimization that reliably favors one isomer over another. By assuming the reaction torque of the motors on the frame is zero and keeping symmetric weighting, the isomers will have identical scalar performance metrics and the optimizer will find exactly two global minima.

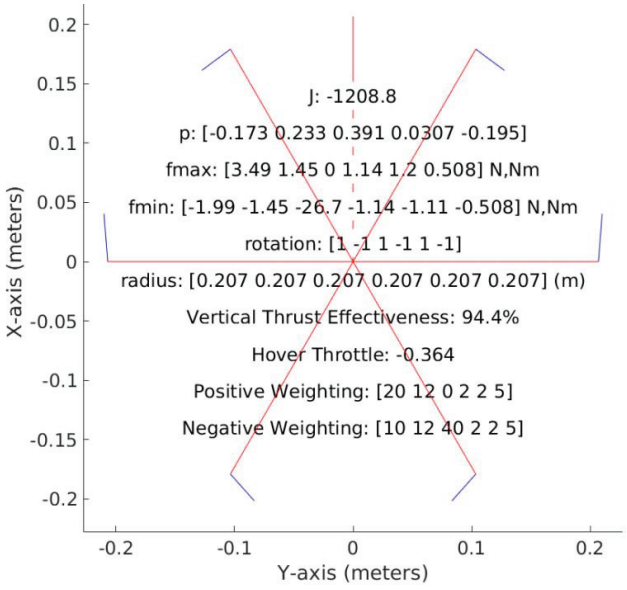

Figure 4. The optimization result plot of the hexrotor case study. The calculated p , f_{max}, f_{min} vectors, length of each motor arm, VTE, and throttle at steady hover are also demonstrated here.

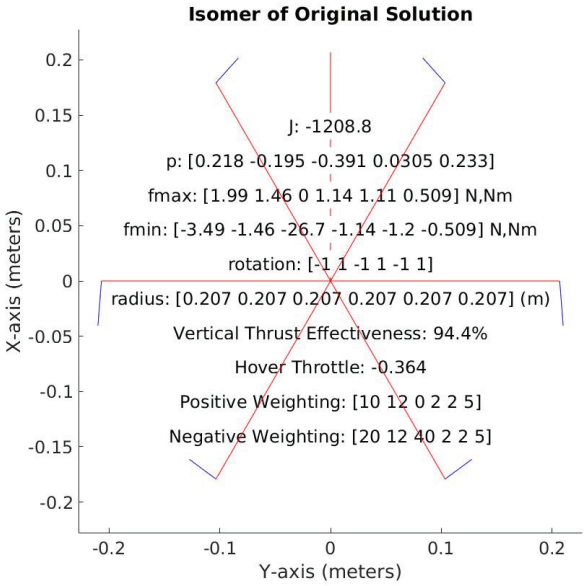

Figure 5. Isomer of the previously presented optimum solution with reversed rotor rotations.

Alternate rotation arrangements are possible with this 6-DoF controllable airframe as motor thrusts dominate the vehicle dynamics and motor torques are not relied on for yaw control authority as is the case with planar rotors layout. However, through our experimenting we have not found an arrangement that offers better performance than the traditional alternating pattern described here.

Versatility of the Optimizer

This paper mostly presents and discusses a case study of a hexrotor design optimization for realizing 6-DoF actuation. However, the possibility for the proposed optimizer to be applied to multirotor UAVs with more or fewer actuators has been explored as well. We present here a preliminary X8 octorotor configuration as in Fig. 6 by expanding the dimensions of search space, mixing matrix and force matrix. Moreover, as mentioned earlier in Sec.§2, although the rotors discussed in the scope of this paper are uni-directional, this optimizer does not discriminate the rotor directions, which means the configuration with actuators providing bi-directional propulsion, e.g. unmanned underwater vehicles, can potentially be optimized as well.

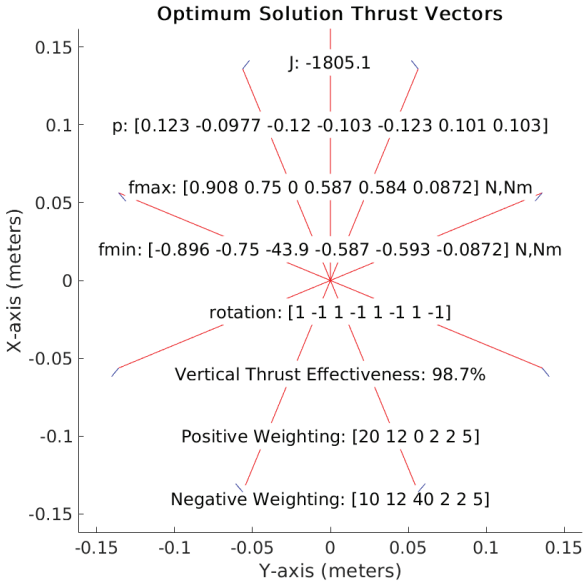

Figure 6. An excursion to utilize the optimizer for X8 octorotor design

4. Comparison with Related Work

This section is to compare the result of our hexrotor case study with some other available fixed-tilt hexrotor configurations in both industries and academia. DJI Technology, one of the world's most successful consumer UAV manufacturers, has released several hexrotor platforms with rotor offset angles including the DJI M600 Pro [24] and the earlier version DJI S1000 [25]. The authors took measurements of the rotor inclination angles of a DJI M600 Pro and listed them together with each rotor's thrust vector in Table 1. The clockwise sequence of rotors is defined using the same convention as shown in Fig. 2. The thrust vectors V_i are the unit vectors indicating the orientation of i-th rotor in the hexrotor's body frame. The angle components ϕ_i and θ_i are defined using the convention in Sec. §**III**. A of [16]. The VTE of DJI M600 Pro is calculated to be 98.8%, and since this system is still under-actuated in flight, the rotor tilting angles here do not serve to generate lateral forces or realize in-hover rotational

maneuvers. DJI M600 Pro embodies a trend in the multi-rotor market over the past few years to tilt the rotors inwards toward the center of the frame. This rotates the force vector of each rotor in such a way as to move the moment created by roll and pitch control inputs closer to the center of mass. This applies only in the traditional layout where the center of mass is below the rotor plane. In our case, the center of mass of a DJI M600 Pro is measured to be $132.08mm$ below the rotor plane.

Table 1. DJI M600 Pro Measurements and Thrust Vectors

Rotor No.	ϕ_i (°)	θ_i (°)	V_i
1	3.1	9.4	$[-0.163, -0.059, -0.985]^T$
2	-1.1	-6.9	$[0.120, -0.019, -0.993]^T$
3	7.5	-5.7	$[0.099, -0.131, -0.987]^T$
4	-7.4	-3.4	$[0.059, 0.129, -0.990]^T$
5	2.3	-8.4	$[0.146, 0.040, -0.989]^T$
6	-3.3	9.3	$[-0.163, 0.058, -0.985]^T$

CyPhy Works [26] proposed a hexrotor capable of flying forward without having to pitch, mitigating the need for a camera gimbal. And as mentioned in Sec.§1, [6], [18] also proposed their rotor optimization approaches and presented their results in both papers. We manage to reconstruct their hexrotor layouts and estimate some of the performance metrics to compare with the result from Optimum.

Based on a CAD rendering from CyPhy Works' website, we derived the rotor orientations of their 6-DOF frame and evaluated the likely performance with our theoretical model. To get a performance comparison, we apply their rotor orientations to the case study frame dimensions and motor parameters which are similar to that of the LVL1 hexrotor. The layout can be seen in Fig.7 and is compared against our optimized solution from Fig.4. By converting the global direction vectors of the angles to local coordinates for the end of each arm, it can be seen that each rotor twists inwards $14.5°$ towards its arm and twists about its arms $15.5°$. This indicates that the angles were probably chosen by intuitively tuning 2 parameters instead of searching over the full range of possible rotor orientations. In Table 2 it can be seen that the Optimum solution has greater maximum control authority than the CyPhy layout in every direction, with a better efficiency in hover. We don't compare the DJI M600 Pro with the other related work here since it is not considered as a fully-actuated system.

Jiang et al.'s Dexterous Hexrotor in [18] optimized the rotors layout over the actuator authorities in X and Y directions of the body frame and efficiency which is equivalent to our VTE. They apllied their layout on a hexrotor with a mass of 2.2 kg and rotot arm of 0.25m, which is heavier and wider compared to our case study. However, since airframe specific parameters sizing and weights were not taken into considerations by them, we can still examine the rotor axes of Dexterous Hexrotor using this case study's parameters without losing generality. They obtained the cant angle and dihedral angle to be $28°$ and $0°$, respectively, which is equivalent to a p-vector of $[-0.235, 0.407, 0.470, 0, -0.235, -0.407]$ in our context. The estimates of its performance metrics are shown in Table 2. These metrics are close to Optimum's forces, torques, and VTE, while Optimum is slightly better in X and Y actuator authorities and VTE.

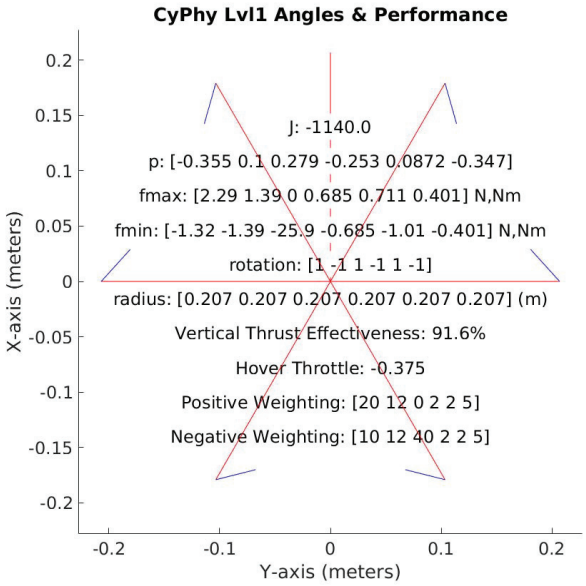

Figure 7. Rotor orientations and corresponding performance characteristics of the CyPhy LVL1 hexrotor.

Rajappa et al.'s hexrotor design in [6] aimed to minimize the control effort by defining the the time integral of the control vector norm as the objective funtion, obtaining a result of $\alpha^* = 0.49$ rad (cant angle) and $\beta^* = 0.33$ rad (dihedral angle). As shown in Table 2, Rajappa's design outperforms in negative X, Y, and yaw authorities while falls behind Optimum's in all others. However, Rajappa's design cannot meet the constraint of $f_{min}[3] \leq -24.329N$, meaning it may face deficiency of vertical lift at low battery voltage.

Table 2. Comparison of the estimated performance metrics

Metrics	**Optimum**	**CyPhy**	**Dexterous**	**Rajappa's**
X(N)	3.49	2.29	3.14	3.42
-X	-1.99	-1.32	-1.90	-2.39
Y	1.45	1.39	1.37	2.60
Z	-26.7	-25.9	-26.2	-23.6
roll(Nm)	1.14	0.69	0.98	0.83
pitch	1.20	0.71	1.13	0.77
-pitch	-1.11	-1.01	-1.13	-1.09
yaw	0.51	0.40	0.63	0.91
VTE	94.4%	91.6%	92.7%	83.5%

5. Experimental Model Validation

For this case study we designed and constructed a hexrotor frame with interchangeable 3D printed motor mounts. We

Figure 8. The thrust testing stand with optimized rotor angles

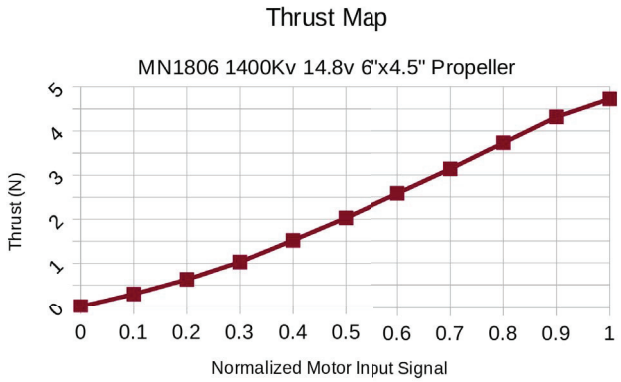

Figure 9. Thrust vs normalized motor input curve from motor-propeller characterization.

utilized an RCbenchmark thrust stand [27] to characterize the motor and propeller combination and to directly measure the available thrust in X and Y. We also used a 2kW DC power supply to drive the single-motor test and the full frame test to ensure varying battery voltages did not effect the result. After finishing the thrust stand tests for single motor-propeller combination as well as the whole hexrotor frame, a flight test is conducted by utilizing a BeagleBone Blue computer [28] as flight controller and a customized power distribution board [29] in order to collect X and Y acceleration data with the on-board sensor to estimate the in-flight thrusts. The constructed frame is pictured in Fig.10.

Motor-Propeller Characterization

The linear model and mixing matrix M assume that the thrust from each motor is proportional to the control inputs. This is not the case with hobby-grade brushless motor and propeller combinations. To account for this it is necessary to linearize the output by correcting the motor thrust curve. This is done by by taking 10 evenly spaced thrust measurements to generate a thrust curve for that specific motor and propeller combination. Nominal battery voltage during flight is 14.8V for this case study. The resulting curve is shown in Fig.9, indicating the characteristics of the combination of T-Motor MN1806 1400Kv brushless DC motor and Hobbypower Nylon 3-Blade 6045 6x4.5 propeller installed on the case study hexrotor.

Within the flight controller we map a desired thrust to an actual signal s_i that will be sent to the motors by linearly interpolating between the two nearest points of our experiment. This is a computationally inexpensive process and keeps the system behaving as linearly as possible.

Hexrotor Thrust Stand Results

The control force vectors f_{min} and f_{max} from Eq.12 predict a maximum control input of $3.49N$ in the $+X$ direction, $1.99N$ in the $-X$ direction, and $1.45N$ in the $\pm Y$ direction.We simulate a hover scenario with all rotors spun up to the hover state s_h with the entire frame fixed to the same thrust test stand used to characterize the motors.We then apply thrust in the $\pm X$ and $\pm Y$ directions. The results are listed in table 3.

Table 3. Comparison of X and Y force performances between theoretical predictions, trust stand data and in-flight IMU data

	$+\mathbf{X}$	$-\mathbf{X}$	$+\mathbf{Y}$	$-\mathbf{Y}$
Predicted (N)	3.49	-1.99	1.45	-1.45
Thrust stand	3.75	-2.32	1.66	-1.64
Flight	3.54	-1.86	1.55	-1.67

While we are pleased to have achieved higher measured thrust in the X and Y directions than the model predicts, we must understand where the error comes from. Firstly, our model does not account for aerodynamic effects due to the interaction of closely spaced rotors. Secondly, we notice that the motors generate approximately 20% greater thrust at room temperature ($\sim$20°C) than when hot ($\sim$60°C). The thermal and aerodynamic properties of the single-motor test cannot be guaranteed to be equal to those of the constructed hexrotor frame.

Table 4. Comparison of pitch, roll and yaw torque performances between theoretical predictions and estimates from in-flight IMU data

	$+\mathbf{Pitch}$	$-\mathbf{Pitch}$	**Roll**	**Yaw**
Predicted (Nm)	1.20	-1.11	1.14	0.51
Flight	1.25	-1.16	1.05	0.56

Flight Test Results

The same hexrotor used in Sec.§5 was removed from the thrust test stand and equipped with landing gear and a camera as in Fig. 10 for flight testing. Utilizing the rc_pilot flight controller [30], the frame was flown with a feedback controller set to keep both roll and pitch angles level at zero degrees in the "Direct Throttle Mode". The the right stick of the radio

controller, which normally maps to roll and pitch angle on a traditional quadcopter, was then mapped to direct inputs to the X and Y translational control directions. Yaw remained controlled by feedback while throttle in the Z direction to maintain altitude was done manually by the pilot.

The pilot performed aggressive step inputs to the system in positive and negative X and Y directions just as was done on the test stand. The force applied to the system is then derived by averaging logged accelerometer readings during flight and multiplying by the known system mass. The X and Y force components calculated from acceleration state estimates are shown in Fig. 11. There were in total 13 experiments performed for positive and negative X forces each, and 6 experiments for positive and negative Y forces each. As listed in table 3, the in-flight force results are

Figure 10. The assembled hexrotor with the optimized rotor configuration from our case study

reasonably close to the test stand results. Here we expect much more error since the condition of steady hover throttle is no longer true while the system is in flight with both the pilot and feedback controllers trying to keep the system level in flight. The fluid flow through and around the rotors can also no be guaranteed to be the same while in flight compared to being fixed to a table.

After the force performances experiments were conducted, an additional series of experiments were designed to estimate the hexrotor's torque performances in flight. The hexrotor is switched to "4-DoF Mode" in order to perform rotations, expected to generate torques around X and Y axes in body frame. Then aggressive step inputs were performed in positive and negative pitch, roll, and yaw directions. The gyroscope data at these aggressive maneuvers were recorded, and the angular accelerations of the hexrotor were estimated using linear regression between time and angular velocity data. Then the maximum and minimum torques were computed using the moments of inertia given in (4). The experimental results are presented in Fig. 11, and the each of averaged torques is compared with the predicted torques. As can be seen in Table 4, the in-flight torques are close to expectations, with the roll torque slightly more deviated. These results are not accurate due to both moments of inertia and angular accelerations are estimated data without direct measurements, while their proximity to the Optimum predictions validates the effectiveness of our optimization approach.

6. Conclusion and Future Work

This paper demonstrates a method for evaluating and optimizing the performance of a fixed-tilt multirotor with direct control authority in all six degrees of freedom. The performance advantage of this control strategy is shown and compared against existing technologies. Furthermore, the qualitative and quantitative effects of multirotor airframe design on optimum rotor orientations and real-world performance are illustrated in theory and in practice resulting in a 3D printed multirotor which matches our performance predictions during physical testing on both a test jig and while in flight. We have begun simulating the airflow and body forces of a soft ducted hexrotor designed with this optimization method for the purpose of safe flight in confined and potentially hazardous environments such as caves and collapsed buildings. In these simulations we find additional stability benefits to the fixed-tilt hexrotor design due to the modified airflow when flying close or adjacent to walls and obstacles. We look forward to sharing these additional findings soon.

Acknowlegments

This work was supported by the National Science Foundation (NSF) under award #DGE-0966375, "Training, Research and Education in Engineering for Cultural Heritage Diagnostics," and award #CNS-1338192, "MRI: Development of Advanced Visualization Instrumentation for the Collaborative Exploration of Big Data." Additional support was provided by the Kinsella Expedition Fund, the Qualcomm Institute at UC San Diego and the World Cultural Heritage Society. Opinions, findings, and conclusions from this study are those of the authors and do not necessarily reflect the opinions of the research sponsors.

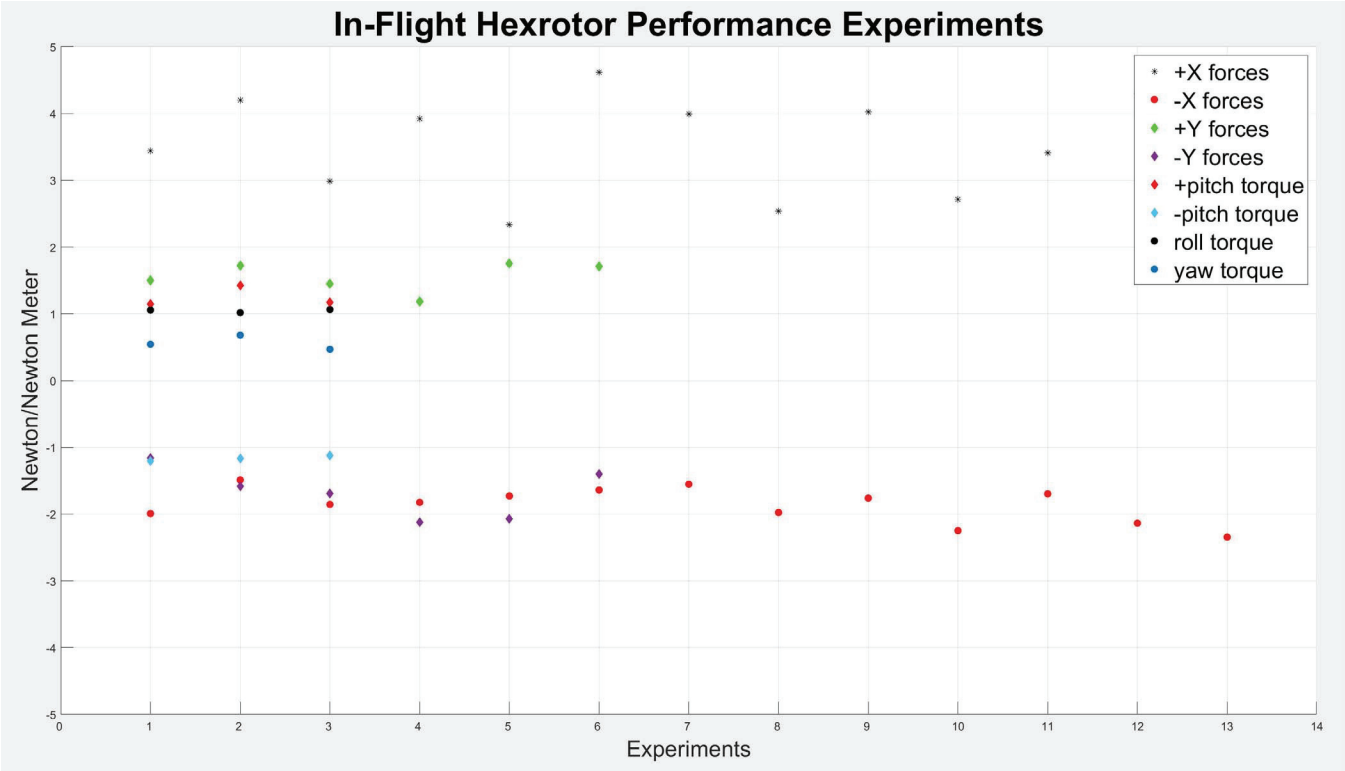

Figure 11. The experimental data of force and torque components in all 6 DoFs, calculated from IMU data.

REFERENCES

[1] Zhaolin Yang, Feng Lin, and B. M. Chen. Survey of autopilot for multi-rotor unmanned aerial vehicles. In *IECON 2016 - 42nd Annual Conference of the IEEE Industrial Electronics Society*, pages 6122–6127, 2016.

[2] S Sankarasrinivasan, E Balasubramanian, K Karthik, U Chandrasekar, and Rishi Gupta. Health monitoring of civil structures with integrated uav and image processing system. *Procedia Computer Science*, 54:508–515, 2015.

[3] AK Puttock, AM Cunliffe, K Anderson, and Richard E Brazier. Aerial photography collected with a multirotor drone reveals impact of eurasian beaver reintroduction on ecosystem structure. *Journal of Unmanned Vehicle Systems*, 3(3):123–130, 2015.

[4] Dominique Meyer, Michael Hess, Eric Lo, Christine E Wittich, Tara C Hutchinson, and Falko Kuester. Uav-based post disaster assessment of cultural heritage sites following the 2014 south napa earthquake. In *2015 Digital Heritage*, volume 2, pages 421–424. IEEE, 2015.

[5] T. Shimizu, S. Suzuki, T. Kawamura, H. Ueno, and H. Murakami. Proposal of 6dof multi-copter and verification of its controllability. *Society of Instrument and Control Engineers of Japan (SICE), 2015 54th Annual Conference of the*, pages 810–815, July 2015.

[6] Sujit Rajappa, Markus Ryll, Heinrich H Bülthoff, and Antonio Franchi. Modeling, control and design optimization for a fully-actuated hexarotor aerial vehicle with tilted propellers. In *2015 IEEE international conference on robotics and automation (ICRA)*, pages 4006–4013. IEEE, 2015.

[7] Markus Ryll, Heinrich H Bülthoff, and Paolo Robuffo Giordano. Modeling and control of a quadrotor uav with tilting propellers. In *2012 IEEE International Conference on Robotics and Automation*, pages 4606–4613. IEEE, 2012.

[8] Markus Ryll, Heinrich H Bülthoff, and Paolo Robuffo Giordano. First flight tests for a quadrotor uav with tilting propellers. In *2013 IEEE International Conference on Robotics and Automation*, pages 295–302. IEEE, 2013.

[9] F. Şenkul and E. Altuğ. Modeling and control of a novel tilt — roll rotor quadrotor uav. In *2013 International Conference on Unmanned Aircraft Systems (ICUAS)*, pages 1071–1076, 2013.

[10] Mina Kamel, S. Verling, O. Elkhatib, C. Sprecher, Paula Wulkop, Z. Taylor, R. Siegwart, and Igor Gilitschenski. Voliro: An omnidirectional hexacopter with tiltable rotors. *ArXiv*, abs/1801.04581, 2018.

[11] Markus Ryll, Davide Bicego, and Antonio Franchi. Modeling and control of fast-hex: A fully-actuated by synchronized-tilting hexarotor. In *2016 IEEE/RSJ International Conference on Intelligent Robots and Systems (IROS)*, pages 1689–1694. IEEE, 2016.

[12] Markus Ryll, Davide Bicego, Mattia Giurato, Marco Lovera, and Antonio Franchi. Fast-hex–a morphing hexarotor: Design, mechanical implementation, control and experimental validation. *arXiv preprint arXiv:2004.06612*, 2020.

[13] Sergio Salazar, Hugo Romero, Rogelio Lozano, and

Pedro Castillo. Modeling and real-time stabilization of an aircraft having eight rotors. In *Unmanned Aircraft Systems*, pages 455–470. Springer, 2008.

[14] D. Brescianini and R. D'Andrea. Design, modeling and control of an omni-directional aerial vehicle. In *2016 IEEE International Conference on Robotics and Automation (ICRA)*, pages 3261–3266, May 2016.

[15] Bill Crowther, Alexander Lanzon, Martin Maya-Gonzalez, and David Langkamp. Kinematic analysis and control design for a nonplanar multirotor vehicle. *Journal of Guidance, Control, and Dynamics*, 34(4):1157–1171, 2011.

[16] Pengcheng Cao, James Strawson, Thomas Bewley, and Falko Kuester. Decoupled translational and rotational flight control designs of canted-rotor hexacopters. In *AIAA Scitech 2021 Forum*, page 1058, 2021.

[17] R. Rashad, J. Goerres, R. Aarts, J. B. C. Engelen, and S. Stramigioli. Fully actuated multirotor uavs: A literature review. *IEEE Robotics Automation Magazine*, 27(3):97–107, 2020.

[18] Guangying Jiang, Richard Voyles, Kenneth Sebesta, and Helen Greiner. Estimation and optimization of fully-actuated multirotor platform with nonparallel actuation mechanism. In *2017 IEEE/RSJ International Conference on Intelligent Robots and Systems (IROS)*, pages 6843–6848. IEEE, 2017.

[19] Evin J. Cramer, Jr. J. E. Dennis, Paul D. Frank, Robert Michael Lewis, and Gregory R. Shubin. Problem formulation for multidisciplinary optimization. *SIAM Journal on Optimization*, 4(4):754–776, 1994.

[20] J.N. Siddall. *Optimal Engineering Design: Principles and Applications*. Dekker Mechanical Engineering. Taylor & Francis, 1982.

[21] M. Faessler, D. Falanga, and D. Scaramuzza. Thrust mixing, saturation, and body-rate control for accurate aggressive quadrotor flight. *IEEE Robotics and Automation Letters*, 2(2):476–482, April 2017.

[22] Brian T Whitehead and Stefan R Bieniawski. Model reference adaptive control of a quadrotor uav. In *AIAA Guidance, Navigation, and Control Conference*, pages 2–5, 2010.

[23] Matlab optimization toolbox, 2020. The MathWorks, Natick, MA, USA.

[24] DJI Technology. Matrice 600pro. `https://www.dji.com/matrice600-pro`. Accessed: 2021-01-14.

[25] DJI Technology. Spreading wings s1000. `https://www.dji.com/spreading-wings-s1000`. Accessed: 2021-01-14.

[26] CyPhy Works. Cyphy works lvl1 drone kickstarter campaign. `https://www.kickstarter.com/projects/1719668770/`. Accessed: 2020-02-29.

[27] RCBenchmark. Rcbenchmark product homepage. `https://www.rcbenchmark.com`. Accessed: 2020-02-29.

[28] BeagleBoard.org. Beaglebone® blue. `https://beagleboard.org/blue`. Accessed: 2020-02-29.

[29] James Strawson. Carrier board for 6 brushless motor controllers in beaglebone form factor, Jun 2018. Accessed: 2020-02-29.

[30] J.R. Strawson. *Feedback Control Driven Mechanical Design Optimization.* PhD thesis, UC San Diego, 2018.

BIOGRAPHY

James Strawson *received his BS and PhD degrees in Mechanical and Aerospace engineering from UCSD where he was a member of both the Coordinated Robotics Laboratory as well as the Calit2 Center of Interdisciplinary Science for Art, Architecture and Archaeology, CISA3. He is a member of the BeagleBoard.org foundation and developed the open source libRobotControl library for Robotics Development in Education and Industry.*

Pengcheng Cao *received his BEng in Energy Engineering from Shandong University, China in 2016 and his MSc in Mechanical Engineering from the University of California, San Diego in 2018. He worked as a project engineer in Value Wholesaler Inc. in Duarte, CA in 2018 and is currently pursuing his Ph.D. in the Department of Mechanical Engineering at UC San Diego under the guidance of Prof. Falko Kuester and Prof. Thomas Bewley. His research interests lie in controls and dynamic systems, robotics, and photogrammetry.*

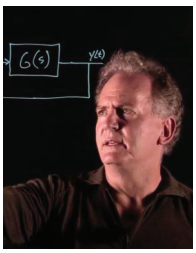

Thomas Bewley *(BS/MS Caltech 1989, PhD Stanford 1998) directs the UCSD Flow Control and Coordinated Robotics Labs, working at the intersection of semi-autonomous agile robotics and the analysis, estimation, and forecasting of environmental flows using advanced control theory and numerical methods.*

Falko Kuester *received an MS degree in Mechanical Engineering in 1994 and MS degree in Computer Science and Engineering in 1995 from the University of Michigan, Ann Arbor. In 2001 he received his PhD from the University of California, Davis and currently is the Calit2 Professor for Visualization and Virtual Reality at the University of California, San Diego. Dr. Kuester holds appointments as Associate Professor in the Departments of Structural Engineering and Computer Science and Engineering and serves as the director of the Calit2 Center of Interdisciplinary Science for Art, Architecture and Archaeology, CISA3.*